Pushing Extended *p*-Quinodimethanes to the Limit: Stable Tetracyano-oligo(*N*-annulated perylene)quinodimethanes with Tunable Ground States

Zebing Zeng,[†] Masatoshi Ishida,[‡] José L. Zafra,[§] Xiaojian Zhu,[∥] Young Mo Sung,[‡] Nina Bao,[⊥] Richard D. Webster,[#] Byung Sun Lee,[‡] Run-Wei Li,[∥] Wangdong Zeng,[†] Yuan Li,[†] Chunyan Chi,[†] Juan T. López Navarrete,[§] Jun Ding,*[,⊥] Juan Casado,*[,§] Dongho Kim,*[,‡] and Jishan Wu*[,†,∇]

[†]Department of Chemistry, National University of Singapore, 3 Science Drive 3, 117543, Singapore

[‡]Spectroscopy Laboratory for Functional π-Electronic Systems and Department of Chemistry, Yonsei University, Seoul 120-749, Korea

[§]Department of Physical Chemistry, University of Malaga, Campus de Teatinos s/n, 229071 Malaga, Spain

[∥]Key Laboratory of Magnetic Materials and Devices, Ningbo Institute of Materials Technology and Engineering, Chinese Academy of Sciences, Ningbo 315201, People's Republic of China

[⊥]Department of Materials Science & Engineering, National University of Singapore, 119260, Singapore

[#]Division of Chemistry & Biological Chemistry, School of Physical & Mathematical Sciences, Nanyang Technological University, 21 Nanyang Link, 637371, Singapore

[∇]Institute of Materials Research and Engineering, A*STAR, 3 Research Link, 117602, Singapore

S *Supporting Information*

ABSTRACT: *p*-Quinodimethane (*p*-QDM) is a fundamental building block for the design of π-conjugated systems with low band gap and open-shell biradical character. However, synthesis of extended *p*-QDMs has usually suffered from their intrinsic high reactivity and poor solubility. In this work, benzannulation together with terminal cyano-substitution was demonstrated to be an efficient approach for the synthesis of a series of soluble and stable tetracyano-oligo(*N*-annulated perylene)-quinodimethanes *n*Per-CN (*n* = 1−6), with the longest molecule having

12 *para*-linked benzenoid rings! The geometry and electronic structures of these oligomers were investigated by steady-state and transient absorption spectroscopy, nuclear magnetic resonance, electron spin resonance, superconducting quantum interference device, and FT Raman spectroscopy assisted by density functional theory calculations. They showed tunable ground states, varying from a closed-shell quinoidal structure for monomer, to a singlet biradical for dimer, trimer, and tetramer, and to a triplet biradical for pentamer and hexamer. Large two-photon absorption cross-section values were observed in the near-infrared range, which also exhibited a clear chain-length dependence.
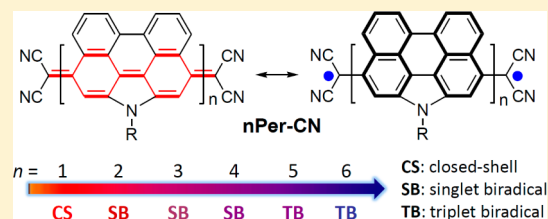
I. INTRODUCTION

p-Quinodimethane (*p*-QDM) (Figure 1) and its biradical form were originally proposed as products in the pyrolysis of *p*-xylene.[1] It has a large biradical character in the ground state due to recovery of the aromaticity of the central benzenoid ring, and thus it is highly reactive. Great efforts have been made to prepare stable *p*-QDM derivatives and its extended analogues. For example, substitution of the terminal methylene sites in *p*-QDM and *p*-dibenzoquinodimethane by four phenyl groups resulted in relatively stable Thiele's hydrocarbon[2] and highly reactive but still characterizable Tschitschibabin's hydrocarbon,[3] respectively. Terminal substitution by cyano group turned out to be another efficient approach, and several stable *p*-QDM derivatives such as 7,7,8,8-tetracyanoquinodimethane (TCNQ),[4] 13,13,14,14-tetracyano-4,5,9,l0-tetrahydro-2,7-pyre-noquinodimethane (TCNTP),[5] and 13,13,14,14-tetracyano-

2,7-pyrenoquinodimethane (TCNP)[5] have been successfully prepared (Figure 1). The tetracyanodiphenoquinodimethane (TCNDQ) without any substitution on the diphenoquinoid moiety (Figure 1), however, could not be isolated as it tended to simultaneously polymerize.[6] The further extension of TCNTP and TCNP frameworks is problematic because of their poor solubility and limited functionalization sites. An alternative approach to extend quinoidimethanes is to replace the benzenoid ring by other heterocycles such as thiophene and thiazole, and some soluble and stable tetracyano-heteroqui-noids[7] have been prepared and used as acceptors in charge-transfer conductors[8] and as semiconductors for *n*-channel or ambipolar field-effect transistors.[9] Among them, a series of
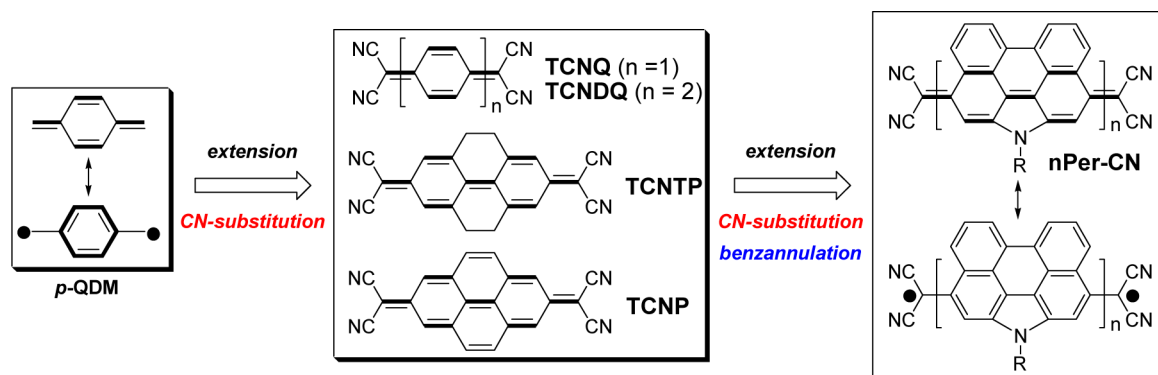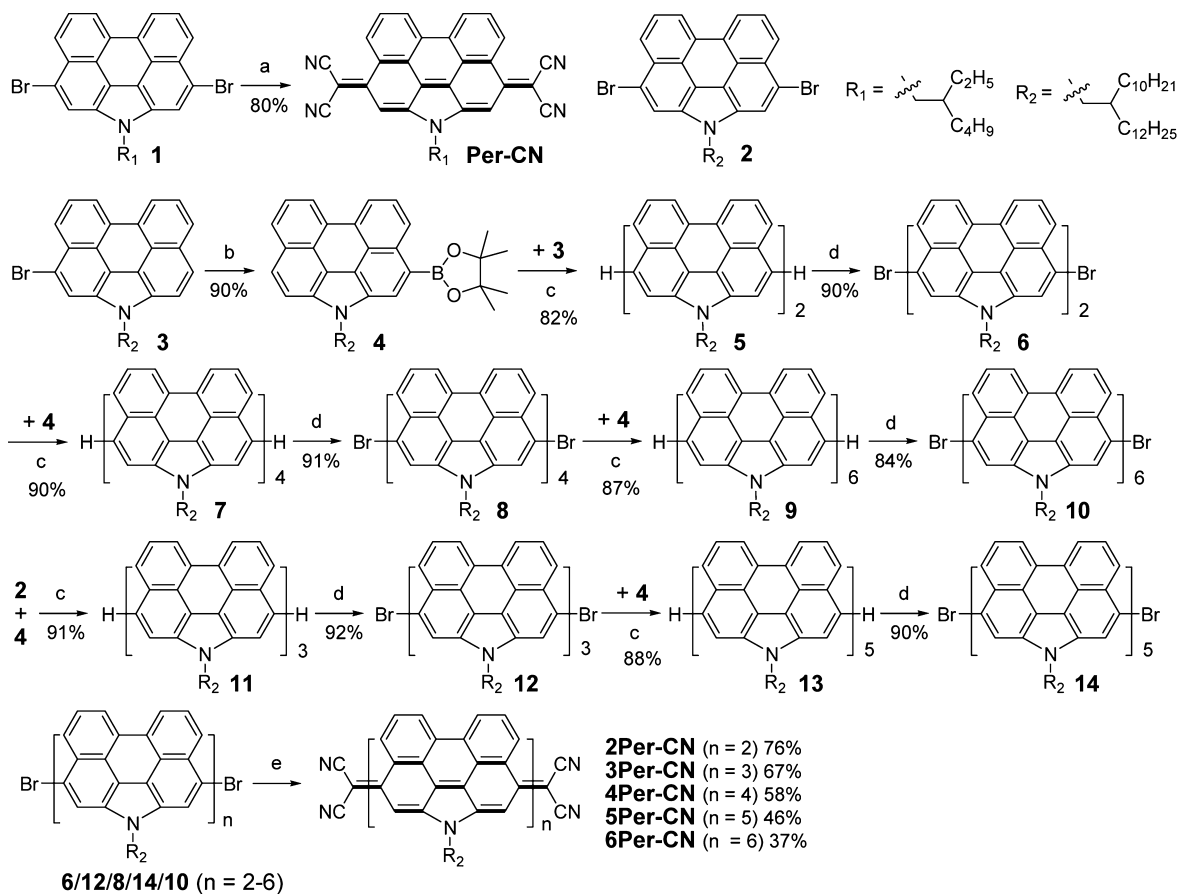
Figure 1. Structural evolution of extended *p*-QDMs.

Scheme 1. Synthesis of *n*Per-CN[a]

[a]Reagents and conditions: (a) (i) malononitrile, NaH, Pd(PPh₃)₂Cl₂, reflux, 48 h; (ii) HCl (2M), air; (b) pinacolborane, PdCl₂(PPh₃)₂, 1,2-dichloroethane/Et₃N, 90 °C, 24 h; (c) Pd(PPh₃)₄, Cs₂CO₃, toluene/DMF, 90 °C, 24 h; (d) NBS (2 equiv), DCM/DMF, 0−25 °C, overnight; (e) (i) malononitrile, NaH, Pd(PPh₃)₂Cl₂, reflux, 48 h; (ii) HCl (2M); (iii) *p*-chloranil, CHCl₃, room temperature.

quinoidal oligothiophenes up to hexamer displayed interesting chain-length dependence of their ground-state electronic structures, with the pentamer and hexamer showing significant singlet biradical character.[10] Incorporation of a *p*-QDM moiety and its analogues such as 2,6-naphthoquinodimthane[11] and 2,6-anthraquinodimethane[12] into a fused π-conjugated framework has proved to be an efficient way to generate polycyclic hydrocarbons with potential open-shell biradical ground states, and typical examples include indenofluorenes,[13] bis-(phenalenyls),[14] and zethrenes.[15] These polycyclic hydrocarbons exhibit unique optical, electronic, and magnetic

properties and have promising applications in nonlinear optics,[16] organic electronics,[17] organic spintronics,[18] and energy storage devices.[19]

Although many useful materials based on *p*-QDM have been prepared and well investigated in recent years, how to make largely extended *p*-QDMs is still a big challenge due to their intrinsic high reactivity arising from their increasing biradical character with extension of their chain length. Solubility of course is another critical concern. Recently, we demonstrated that benzannulation is an efficient approach to stabilize the highly reactive Tschitschibabin's hydrocarbon.[20] Inspired by

this success, in this research we demonstrate that by using a *N*-annulated perylene (NP) as a building block, we are able to prepare a series of soluble and stable oligo(*N*-annulated perylene)quinodimethanes *n***Per-CN** (*n* = 1−6), with the longest molecule having 12 *para*-linked benzenoid rings (Figure 1). The NP was chosen on the basis of the following considerations: (1) the quinoidal NP can be regarded as a structure where the *p*-diphenoquinoid is annulated by two aromatic benzene rings, and thus stability will be improved; (2) flexible alkyl chain can be easily attached to the N-site and thus resolve the solubility problem; and (3) selective functionalization can be easily conducted at the *peri*-edges of NP and allows us to prepare higher order oligomers.[21] In addition, the electron-withdrawing cyano-groups at the terminal methylene sites will further stabilize the systems. The ground-state geometry and electronic structure of these oligomers were systematically investigated by steady-state absorption and transient absorption (TA), variable-temperature (VT) nuclear magnetic resonance (NMR), electron spin resonance (ESR), superconducting quantum interference device (SQUID) measurements, and FT Raman spectroscopy assisted by density functional theory (DFT) calculations. Our research disclosed interesting chain-length dependence of their ground states and optical, electrochemical, and magnetic properties.

II. RESULTS AND DISCUSSION

Synthesis. As shown in Scheme 1, all of the target compounds *n***Per-CN** (*n* = 1−6) were prepared by Takahashi coupling[22] from the corresponding dibromo-oligo(*N*-annulated perylenes), followed by oxidative dehydrogenation. For the monomer **Per-CN**, short alkyl substituent (2-ethylhexyl) can provide sufficient solubility. However, for higher oligomers *n***Per-CN** (*n* = 2−6), a long branched dove-tailed chain (2-decyltetradecyl) has to be employed to ensure sufficient solubility for the intermediates and final products. The dibromo-NPs **1** and **2** and the monobromo-NP **3** were first synthesized by controlled bromination with *N*-bromosuccinimide (NBS) according to previous reports.[21] Pd-catalyzed Takahashi coupling of **1** with malononitrile in the presence of sodium hydride in anhydrous THF worked smoothly and afforded the **Per-CN** as a deep blue solid in 80% yield after acidification and simultaneous oxidation in air. The higher order oligomers were synthesized by repetitive Suzuki coupling/bromination reactions. The NP monoboronic ester **4** as a key intermediate was prepared by Miyaura borylation reaction from **3**. Suzuki coupling between **3** and **4** gave the NP dimer **5**, which was brominated with NBS to afford the dibromo-NP dimer **6**. Suzuki coupling between **6** and **4** generated NP tetramer **7**, and subsequent bromination provided the dibromo-NP tetramer **8**. Similar Suzuki coupling/bromination protocol from **8** gave the dibromo-NP hexamer **10**. The dibromo-NP trimer **12** was prepared by Suzuki coupling between **2** and **4**, followed by bromination with NBS. Subsequent Suzuki coupling with **4** and bromination afforded the dibromo-NP pentamer **14**. The quinoidal oligomers *n***Per-CN** (*n* = 2−6) were then prepared in tens of milligram scale by similar Takahashi coupling reaction from the corresponding dibromo-NP oligomers (**6**, **12**, **8**, **14**, and **10**) followed by oxidation with *p*-chloranil in chloroform in 76−37% yields. In these cases, oxygen in air can only oxidize the dihydro-intermediates very slowly; thus a stronger oxidant such as *p*-chloranil has to be used to ensure a complete dehydrogenation. All of the target molecules *n***Per-CN** are

soluble in common organic solvents such as chloroform, toluene, and THF. The compounds were stable enough to be readily obtained as analytically pure products in both solid and solution except that the hexamer **6Per-CN** in solution was moderately sensitive to light and it partially decomposed on silica gel column, which prevented us from separating even longer oligomers. All of the intermediates were well characterized by ^{1}H and ^{13}C NMR and mass spectrometry (MS), and the purity of the final products was confirmed by high-resolution MS and by high performance liquid chromatography (HPLC) (see the Supporting Information).

Magnetic Properties. The ^{1}H and ^{13}C NMR spectrum of the smallest derivative, **Per-CN**, in CDCl$_3$ at 298 K exhibits well-resolved resonance signals, indicating that **Per-CN** has a closed-shell quinoidal structure in the ground state. In contrast, the higher *n***Per-CN** (*n* = 2−6) showed NMR silence even at low temperature (−100 °C in CD$_2$Cl$_2$), indicating that these extended quinodimethanes derivatives have a large biradical character in the ground state (vide infra). Accordingly, ESR measurements of all samples except **Per-CN** displayed featureless broad signals in both solid state and solution centered with g_e = 2.0031 (Figure S1 in the Supporting Information). The signal broadening and absence of $\Delta M_s = \pm 2$ forbidden transitions would be due to the long-distance spin−spin dipole interaction within the molecules and the extended spin-delocalization.[14,15e,f] The VT ESR measurements for the powders of *n***Per-CN** (*n* = 2−6) disclosed the significant temperature dependency of the signal intensities; the intensity decreased with decreasing temperature for **2Per-CN**−**4Per-CN**, indicating that they all have a singlet biradical ground state, which is in equilibrium with a higher energy triplet biradical state. The change however became rather slight for **4Per-CN** as compared to that of **2Per-CN**. The trend reversed in case of **5Per-CN** and **6Per-CN**; that is, the ESR intensity increased when lowering the temperature. This infers that the biradicals in the higher oligomers behave more like two individual radicals, presumably due to the very weak coupling through a long distance between two unpaired electrons.

The singlet−triplet energy gap ΔE_{S-T} (i.e., $-2J/k_B$) was estimated by SQUID measurements on the powder form of *n***Per-CN** (*n* = 2−6) at 5−300 K by means of careful fitting of the curves by the Bleaney−Bowers equation[23] (Figure 2 and
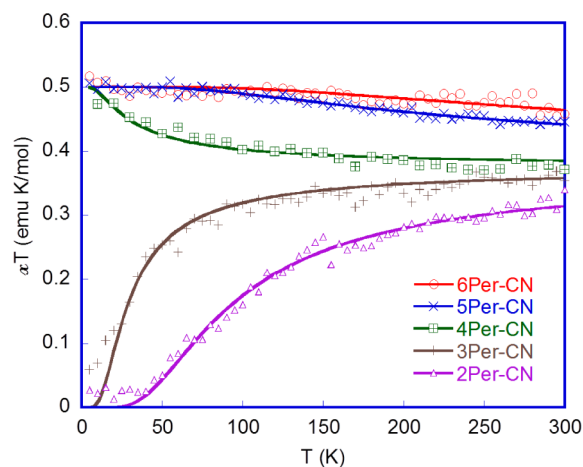

Figure 2. $\chi T - T$ curves in the SQUID measurements for the powder of *n***Per-CN** (*n* = 2−6). The solid lines are the fitting curves according to Bleaney−Bowers equation; *g*-factor was taken to be 2.

Table 1. Photophysical and Electrochemical Data of nPer-CN[a]

compd	λ_{abs} (nm)	ε_{max} ($M^{-1} cm^{-1}$)	τ (ps)	$\sigma^{(2)}_{max}$ (GM)	$E^r_{1/2(ox)}$ (V)	$E^r_{1/2(red)}$ (V)	HOMO (eV)	LUMO (eV)	E_g^{EC} (eV)	E_g^{opt} (eV)	ΔE_{S-T} (kcal/mol)
Per-CN	579	61 400	17.2	1300[b]		−0.54		−4.26		1.74	
	626	66 000				−0.78					
						−1.5					
2Per-CN	351	20 230	8.6	1060[c]	0.36	−0.45	−5.11	−4.50	0.61	0.89	0.342
	620	28 300			0.54						
	901	54 700									
3Per-CN	451	34 800	3.5	770[c]	0.35	−0.41	−5.05	−4.52	0.53	0.93	0.107
	635	67 600			1.0						
	930	22 600									
4Per-CN	460	72 200	3.1	710[c]	0.31	−0.44	−5.05	−4.53	0.52	0.93	−0.064
	635	70 800			0.80						
	930	21 400									
5Per-CN	466	84 900	2.9	730[c]	0.30	−0.45	−5.04	−4.47	0.57	0.93	−0.556
	635	59 600			0.89						
	929	17 300									
6Per-CN	469	10 4400	2.7	710[c]	0.30	−0.43	−5.03	−4.50	0.53	0.93	−0.883
	634	45 400			0.84						
	927	13 000									

[a]λ_{abs}: absorption maximum measured in THF. ε_{max}: molar extinction coefficient at the absorption maximum in the unit of $M^{-1} cm^{-1}$. τ is singlet excited lifetime obtained from TA. $E_{1/2}^{ox}$ and $E_{1/2}^{red}$ are half-wave potentials of the oxidative and reductive waves, respectively, with potentials vs Fc/Fc$^+$ couple. HOMO and LUMO energy levels were calculated according to equations: HOMO $= -(4.8 + E_{ox}^{onset})$ and LUMO $= -(4.8 + E_{red}^{onset})$, where E_{ox}^{onset} and E_{red}^{onset} are the onset potentials of the first oxidative and reductive redox wave, respectively. E_g^{EC}: electrochemical energy gap derived from LUMO−HOMO. E_g^{opt}: optical energy gap derived from lowest energy absorption onset in the absorption spectra. ΔE_{S-T}: singlet−triplet energy gap estimated from SQUID measurements. [b]$\sigma^{(2)}_{max}$ is the maximum TPA cross section at the wavelength of 1200 nm. [c]$\sigma^{(2)}_{max}$ is the maximum TPA cross section at the wavelength of 1700 nm.

Table 1). The ΔE_{S-T} values were estimated as 0.342 and 0.107 kcal/mol for **2Per-CN** and **3Per-CN**, respectively, further confirming that both compounds have a singlet biradical ground state, with the two unpaired electrons weakly coupled. Such small ΔE_{S-T} values allow the facile thermal excitation to the higher energy triplet biradical state. A very small ΔE_{S-T} (−0.064 kcal/mol) was estimated for **4Per-CN**, indicating very weak coupling between the two radicals. Given the unavoidable error during the data fitting for this borderline molecule, the ground state of **4Per-CN** is better described as a singlet biradical with very large biradical character based on the VT ESR measurements, which is also in agreement with DFT calculations to be discussed later. In passing from **4Per-CN** to **5Per-CN** and **6Per-CN**, the ΔE_{S-T} became −0.56 and −0.88 kcal/mol, respectively, implying a triplet biradical ground state. However, considering the long distance between the two radicals, these two compounds may be better described as two individual radicals.

Raman Characterizations. Raman spectroscopy is a unique tool to evaluate the electronic ground state of conjugated biradicals and to understand macroscopic magnetic and optical data with molecular level information.[10b,15f,20,24] To warrant a maximum population of the ground electronic state, either singlet or triplet, the FT-Raman spectra of the nPer-CN samples were recorded at −180 °C (Figure 3). For **Per-CN**, the Raman bands at 1705, 1600, and 1458 cm^{-1} are clearly associated with the quinoidal structure (C=C stretching modes) between the two dicyano groups corroborating its singlet closed-shell nature. In **2Per-CN**, the Raman spectrum experiences a frequency down-shift of the above three important bands toward 1687, 1584, and 1441 cm^{-1}, respectively. This spectroscopic feature reflects the weakening of the C=C bond strength of the quinoidal path due to the recovery of aromatic-like rings for the perylene units. This
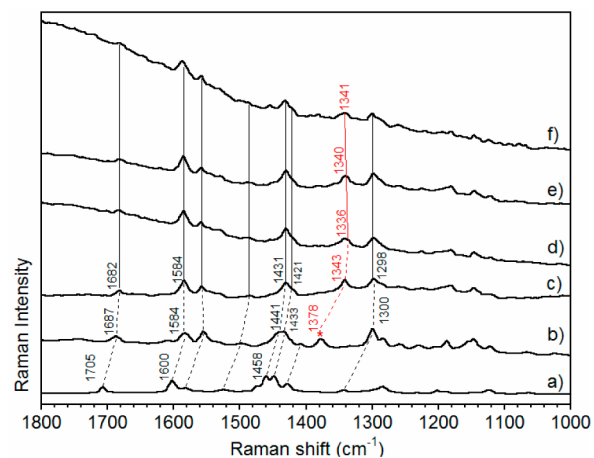

Figure 3. FT-Raman spectra of the nPer-CN at −180 °C in the solid state: (a) **Per-CN**; (b) **2Per-CN**; (c) **3Per-CN**; (d) **4Per-CN**; (e) **5Per-CN**; and (f) **6Per-CN**.

quinoid-to-aromatic tuning of the molecular backbone is the molecular confirmation of the formation of biradical species in **2Per-CN**. From **Per-CN** to **2Per-CN**, a new band appeared at 1378 cm^{-1} due to the creation of the CC interperylene stretching mode with a predominant single C−C character further affirming its biradicaloid state. From **2Per-CN** to **3Per-CN**, the characteristic FT-Raman bands were further downshifted because of increased aromatic stabilization by the incorporation of an additional perylene unit, which reveals a more remarkable biradical character of the molecular framework. The frequency down-shift of the interperylene (C−C) modes (by 35 cm^{-1}) is particularly noticeable because it overexpresses the aromatic character of the open-shell structure of the ground electronic state of **3Per-CN**. However, this large

biradical aromatization incorporates backbone flexibility (constrained in quinoidals structures), which produces interperylene dihedral rotations easily fuelled by steric crowing. Acting together, the planar distortions and the strong perylene aromatization clearly account for the large -35 cm^{-1} displacement. In going from **3-PerCN** to **4-PerCN**, the interperylene C−C stretch down-shifts by 7 cm^{-1}, indicating that the distortive effect increased and conjugation (aromatization) decreased (increased). From **4-PerCN** to **5Per-CN** and **6Per-CN**, the spectra remained unchanged in frequencies, and their spectral profiles were essentially identical. This might indicate that molecular conjugation is already saturated in **4-PerCN** and interperylene rotations are fully relaxed. This molecular spectroscopic information is relevant because saturation of conjugation confines its effect to the molecular center (equivalent to ∼4 NP units) of **5Per-CN** and **6Per-CN** decoupling the two radical centers and deactivating the double spin polarization effect that produces the stabilization of the triplet state in the two largest molecules. In other words, conjugation length (CL) in **5Per-CN** and **6Per-CN** is smaller than the molecular length (ML) supposing a transition from a singlet biradical ground electronic state (CL ≈ ML in **2Per-CN**, **3Per-CN**, and **4Per-CN**) to a triplet ground electronic state (CL < ML in **5Per-CN** and **6Per-CN**).

From a viewpoint of molecular structures, quinoidal *n*Per-CN may exist as cis/trans isomers. For example, the two NP units in quinoidal **2Per-CN** could adopt a *trans*- or a *cis*-configuration through the ethylene linkage (Figure 4a). However, its corresponding biradical resonance form may interconvert them by rotating along the single C−C bond. To identify cis/trans isomerization, IR and Raman spectroscopies can be used invoking the mutual exclusion principle, which is
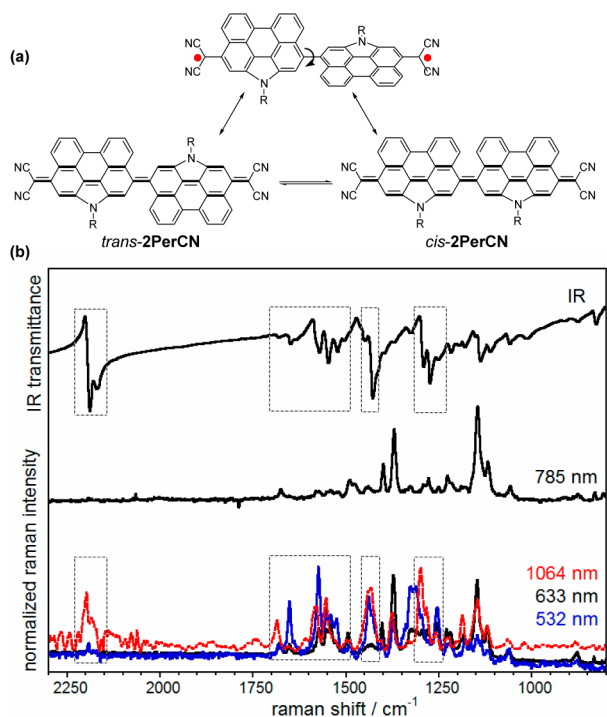
verified in molecules that contain an inversion center among the operations of symmetry, for example, in *trans*-**2Per-CN** (i.e., C_{2h}). The Raman spectra excited at 785 nm and the infrared spectra of **2Per-CN** are clearly complementary (Figure 4b), meaning that those bands especially active in infrared are weakly active or inactive in Raman, and vice versa. This suggests that **2Per-CN** in its ground electronic state is mostly in the *trans*-form between its two NP units. However, by exciting with the 532/1064 nm Raman lasers, the corresponding spectra did not strictly follow the IR/Raman complementary rule (Figure 4b), which suggests that there could exist in **2Per-CN** a certain quantity of *cis*-isomer (C_{2v} molecular symmetry). Thus, the infrared signal averages all possible isomers, while the Raman spectrum, with different excitation wavelengths, can selectively probe one or the other isomer even in minority. The presence of a significant fraction of *cis*-isomer in **2Per-CN** might result from the high energy barrier required to overcome the perpendicular transition state imposed by the medium biradical character. In this regard, for the larger molecules, the progressive interperylene C−C bonds weakening will decrease the cis−trans energy barrier facilitating the dominance of the all-*trans* conformer, which is the disposition that better mitigates steric repulsions.

Optical Properties. This series of *n*Per-CN used in this study exhibit different one-photon absorption (OPA) spectral features as the number of rylene core increased (Figure 5 and Table 1). The monomer **Per-CN** displayed an intense absorption band with maximum at 626 nm (log ε = 4.82; ε: molar extinction coefficient in M^{-1} cm^{-1}), along with a shoulder at 579 nm, which is relatively similar to that of TCNP (λ_{max} = 557 nm, log ε = 4.12).[5] In contrast, the absorption spectrum of **2Per-CN** consisted of three major absorption bands appearing with absorption maxima at 351, 620, and 901 nm, respectively. The characteristic structured long-wavelength absorption bands were observed in the near IR region extending up to 1400 nm, with a very small optical energy gap of 0.89 eV. Such remarkable red-shift of the lowest excitation band and the band shape change as compared to **Per-CN** imply a transformation of their electronic ground state. The trimer **3Per-CN** also showed a very broad near IR band extending to 1400 nm as observed in **2Per-CN** and relatively intense band with λ_{max} of 635 nm in the visible region. This optical feature is entirely seen in further higher *n*Per-CN (*n* = 4−6). Notably, it was found that the wavelengths of lowest transition band are not further extended despite the extension of chain length, and the relative intensity of higher energy bands emerged around 450−470 nm are remarkably enhanced upon the number of rylene core increases in *n*Per-CN. This characteristic band around 450−470 nm may originate from the absorption of aromatic NP cores,[25] which indicates the recovery of the aromatic-like rylene cores by means of perturbation of the quinoidal electronic structures of higher *n*Per-CN associated with terminal spin localization.

Femtosecond TA measurements were carried out to explore the excited-state dynamics of *n*Per-CN (Figure 6, Table 1, and Figure S2 in the Supporting Information). The TA spectrum of **Per-CN** exhibited a ground-state bleaching (GSB) signal around 628 nm, as well as a small excited-state absorption (ESA) band in the 450−510 nm spectral region. The decay profiles probed at 628 nm were fitted by two exponential functions of 2.7 and 17.2 ps. This short singlet excited state lifetime of **Per-CN** is well in agreement with the nonfluorescent properties. In the case of open-shell derivative, **2Per-CN**, one

Figure 4. (a) An equilibrium between *cis*- and *trans*-**2Per-CN** via a biradical transition state; and (b) FT infrared and Raman spectra of **2Per-CN** in the solid state at different excitation wavelengths (532, 633, 785, and 1064 nm).
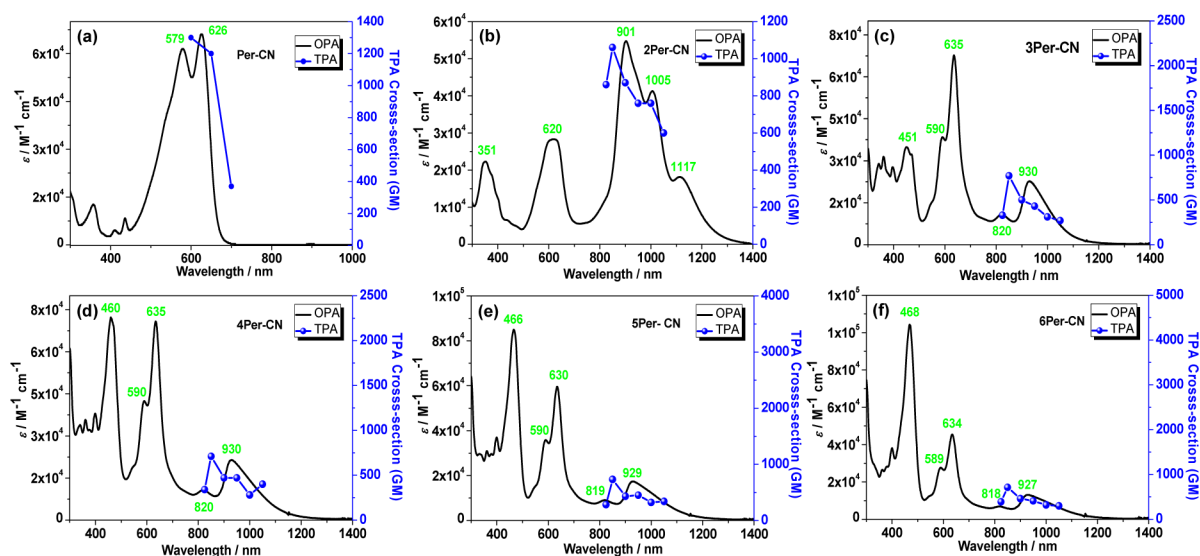
Figure 5. One-photon and two-photon absorption spectra of *n*Per-CN. The spectra were recorded in chloroform and THF, respectively: (a) **Per-CN**; (b) **2Per-CN**; (c) **3Per-CN**; (d) **4Per-CN**; (e) **5Per-CN**; and (f) **6Per-CN**.
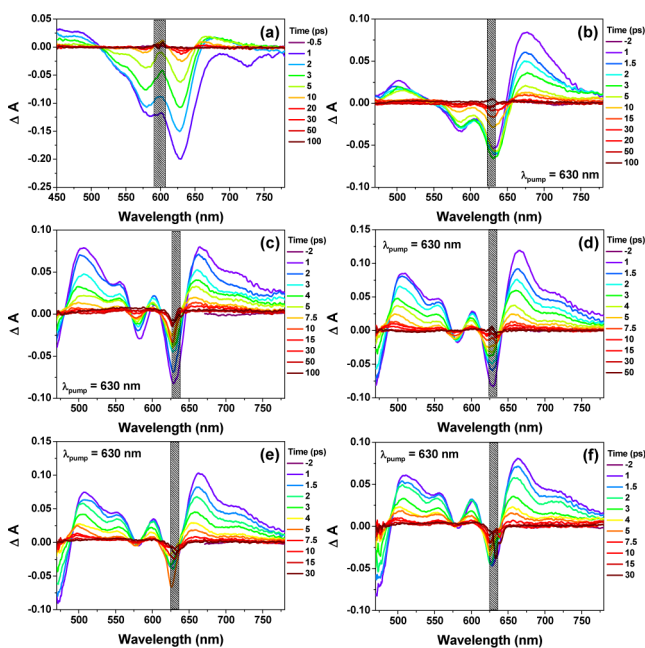

Figure 6. Femtosecond transient absorption spectra of *n*Per-CN measured in tetrahydrofuran at room temperature (296 K): (a) **Per-CN**; (b) **2Per-CN**; (c) **3Per-CN**; (d) **4Per-CN**; (e) **5Per-CN**; and (f) **6Per-CN**.

distinct GSB signals around 550−650 nm and two relative higher intensity ESA bands in spectral regions similar to those of **Per-CN** were observed, with a shorter excited-state lifetime of 8.6 ps. This fast decay kinetic profile of **2Per-CN** is considered to reflect an acceleration of the nonradiative internal conversion rates arising from the smaller energy gap between the lowest excited state and the open-shell ground state. The TA spectra of further higher *n*Per-CN (*n* = 3−6) demonstrated similar spectral features; two major ESA bands in the 480−570 and 645−780 nm regions were observed with shorter singlet excited lifetimes of 2.7−3.5 ps. Considering the similar optical energy gaps among these derivatives estimated in steady-state absorption spectra, this kinetic trend of fast decay of the excited

state could be due to the molecular flexibility with the larger rylene arrays.

As it is known that an open-shell (singlet) biradical character can enhance the two-photon absorption activity,[15f,16,20] TPA measurements were conducted for *n*Per-CN by using the open-aperture Z-scan method to clarify the structure−TPA relationship (Figure 5, Table 1, and Figure S3 in the Supporting Information). The excitation wavelength was scanned in the near IR region from 1200 to 2100 nm where one-photon absorption contribution is negligible. Large TPA cross sections were observed for the closed-shell **Per-CN** with the maximum value of $\sigma^{(2)}$ = 1300 GM at 1200 nm, which could be due to that the quinoidal molecular structures bearing fluctuated atomic bonds may have larger hyperpolarizabilities.[26] As expected, open-shell higher *n*Per-CN also exhibited strong TPA response in the region of 1650−2100 nm, with the maximum TPA cross-section values of $\sigma^{(2)}$ = 1060, 770, 710, 730, and 710 GM, respectively, observed at 1700 nm. In comparison with typical hydrocarbon chromophores, relatively larger cross sections in NIR region were obtained. This trend of $\sigma^{(2)}$ may be correlated to the resonance enhancement of the transitions observed in OPA spectra and the degree of their biradical characters, because the intermediate biradical indices have proved to enhance the second hyperpolarizability (γ), which is the origin of the third-order nonlinear optical (NLO) properties.[27] This result demonstrates the important insights into the correlation between a biradical character index and structural backbones to enhance the TPA property.

Electrochemical Properties. Cyclic voltammetry and differential pulse voltammetry measurements were performed to investigate the electrochemical properties of these oligomers (Figure 7, Table 1, and Figure S4 in the Supporting Information). Most of the compounds displayed multiple chemically reversible reductive and/or oxidative electron transfer processes, indicating that the reduced/oxidized states survived fully or partially on the voltammetric time scale (which is for at least a few seconds). **Per-CN** in dichloromethane exhibited two chemically reversible reductive processes with half-wave potentials $E^r_{1/2}$ = −0.54 V and $E^r_{1/2}$ = −0.78 V. The $E^r_{1/2}$-values were determined from the midpoint of the anodic (E_p^{ox}) and cathodic (E_p^{red}) peak potentials [$E^r_{1/2}$ = (E_p^{ox} +
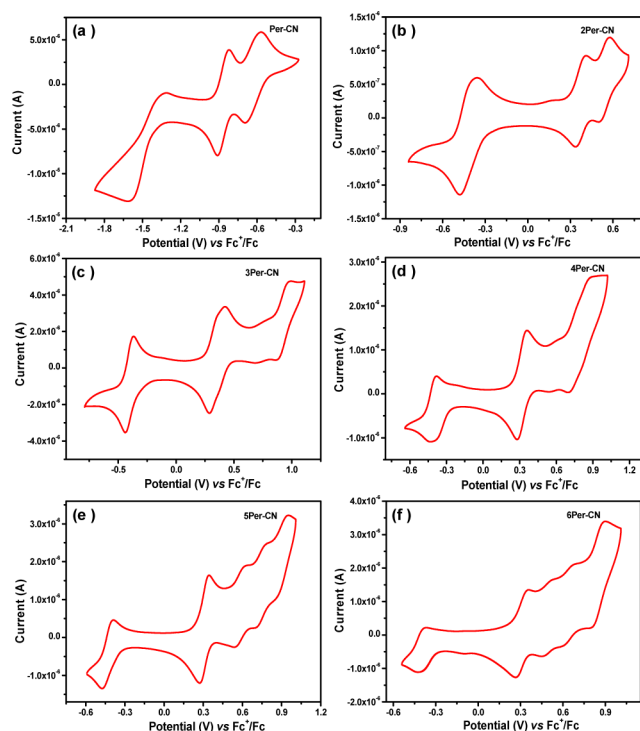
Figure 7. Cyclic voltammograms of (a) **Per-CN**; (b) **2Per-CN**; (c) **3Per-CN**; (d) **4Per-CN**; (e) **5Per-CN**; and (f) **6Per-CN** in dry dichloromethane with 0.1 M Bu_4NPF_6 as supporting electrolyte, Ag/AgCl as reference electrode, Au disk as working electrode, Pt wire as counter electrode, and scan rates at 100, 20, 20, 20, 20, and 20 mV/s, respectively.

$E_p^{red})/2]$ when the anodic (i_p^{ox}) to cathodic (i_p^{red}) peak current ratios were equal to unity $(i_p^{ox}/i_p^{red} = 1)$. **Per-CN** showed another reduction process at more negative potentials $(E_{1/2}^{r} \approx -1.5$ V vs Fc/Fc$^+$) where the i_p^{ox}/i_p^{red}-ratio was <1 (at a scan rate of 100 mV s^{-1}), indicating that the highly reduced state was relatively short-lived. The i_p^{red}-value for the most negative reduction process of **Per-CN** was much greater than the two less negative processes, indicating that more electrons were transferred. No oxidative wave was observed for neutral **Per-CN**. All of the other compounds (**2Per-CN** to **6Per-CN**) could be reduced in one chemically reversible process (or partly chemically reversible process) at negative potentials and oxidized in at least two processes at positive potentials, but with the oxidation processes displaying varying degrees of chemical reversibility. **2Per-CN** was electrochemically oxidized in two chemically reversible processes at $E_{1/2}^{r} = 0.36$ V and $E_{1/2}^{r} = 0.54$ V vs Fc/Fc$^+$, together with one chemically reversible reduction process at $E_{1/2}^{r} = -0.45$ V vs Fc/Fc$^+$, with the reduction process showing twice the peak current of each oxidation process (indicating the transfer of a higher number of electrons). **3Per-CN** exhibited a chemically reversible oxidative process at $E_{1/2}^{r} = 0.35$ V vs Fc/Fc$^+$ (consisting of two closely overlapping peaks) and another oxidation process at $E_{1/2}^{r} \approx 1.0$ V vs Fc/Fc$^+$ (where the i_p^{ox}/i_p^{red}-ratio >1), together with one chemically reversible reductive process at $E_{1/2}^{r} = -0.41$ V vs Fc/Fc$^+$. A similar CV profile was observed for **4Per-CN**, with one chemically reversible oxidation process at $E_{1/2}^{r} = 0.31$ V vs Fc/Fc$^+$, one oxidation process at ~0.80 V vs Fc/Fc$^+$, and one reduction process at $E_{1/2}^{r} = -0.44$ V vs Fc/Fc$^+$. For **5Per-CN** and **6Per-CN**, two major oxidation processes and one reduction process were detected, at potentials similar to those

observed for **3Per-CN** and **4Per-CN**. However, two additional oxidation processes with much smaller peak currents (indicating the transfer of lesser numbers of electrons) were also detected at potentials between the two major oxidation processes. A summary of the half-wave potentials is provided in Table 1. In situations where the i_p^{ox}/i_p^{red}-ratios were different from unity, the reversible half-wave potentials are difficult to determine accurately, and thus the reported $E_{1/2}^{r}$-values are only approximate. Rather low electrochemical energy gaps were estimated for n**Per-CN** ($n = 2-6$) as 0.61, 0.53, 0.52, 0.57, and 0.53 eV, respectively. Such chain-length dependence of electrochemical behavior must be correlated to the change of π-conjugation and electronic structure in these extensive homologues.

Theoretical Calculations. DFT (B3LYP) and 6-31G(d,p) basis set calculations were carried out to establish a better understanding of the spectral and magnetic findings obtained in a series of n**Per-CN** (see details in the Supporting Information). Limited by the computation capacity, the calculation was performed for only shorter derivatives, **Per-CN** up to tetramer **4Per-CN**. For the shortest oligomer **Per-CN**, a closed-shell structure was predicted as the ground state, agreeing with all experimental results (Figure S5 in the Supporting Information). The energy of the triplet state (TB) is higher by +16.36 kcal/mol than that of the singlet (closed shell (CS)/biradical (SB)) solutions. As it is expected, the open-shell SB states of **2Per-CN** obtained by using an unrestricted broken-symmetry wave function method (BS-UB3LYP/6-31G(d,p)) turned out to have the lowest energy than those of the corresponding CS and TB one, and the singlet−triplet energy gaps (ΔE_{SB-TB}) were estimated to be 0.755 kcal/mol, which is close to the experimental values (e.g., 0.342 kcal/mol for **2Per-CN**) (Figure S6 in the Supporting Information). From the structural point of views in **2Per-CN**, the energy of *trans*-isomer can be possibly considered as an energetic minimum geometry in the ground state. The small energy difference (0.377 kcal/mol) between the *trans*- and *cis*-forms leads us to consider that each geometry can be easily interconverted through free rotation of C−C bonds, which is consistent with the vibrational Raman observations (Figure S7 in the Supporting Information). Thus, the higher oligomeric n**Per-CN** ($n = 3-4$) were calculated as all *trans*-forms, which supported the ground-state singlet biradical structures with further smaller ΔE_{SB-TB} of 0.042 and 0.002 kcal/mol, respectively (Figures S8 and S9 in the Supporting Information). With decreasing distinct singlet−triplet energy gaps, it is noteworthy that the singlet biradical character (y) of n**Per-CN** ($n = 2-4$) estimated by the CASSCF(2,2)/6-31G calculation[28] gave larger LUMO occupation numbers of 0.85, 0.99, and 0.99, respectively. These larger (almost saturated: $0 < y < 1$) biradical characters for higher series are well consistent with the experimental observations of distinct magnetic susceptibility behaviors.

As in the investigation of the molecular geometries and the frontier molecular orbitals, a typical disjointed feature in the singly occupied molecular orbital (SOMO) profiles of the biradical species was found; the unpaired electrons (α and β) were mainly delocalized at the backbone of terminal rylene units bearing malononitrile groups (Figures S10−S12 in the Supporting Information). Accordingly, large spin densities on the terminal malononitrile-substituted rylene units in the n**Per-CN** are retained with antiparallel spin electron patterns (Figure 8). The electronic structure of **2Per-CN** in a ground state is

6369

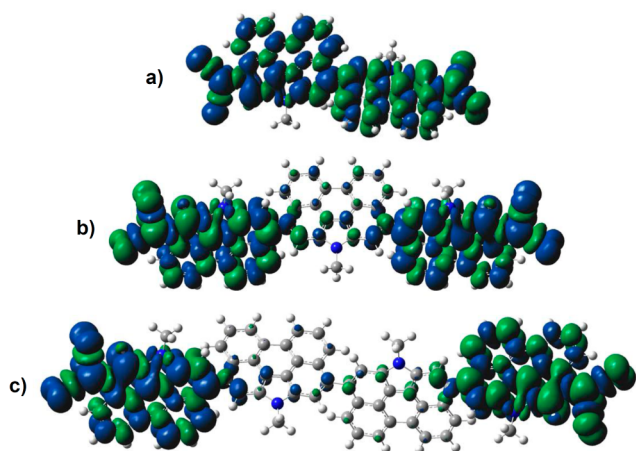dx.doi.org/10.1021/ja402467y | *J. Am. Chem. Soc.* 2013, 135, 6363−6371

Figure 8. Calculated (UB3LYP) spin density distribution: (a) **2Per-CN**; (b) **3Per-CN**; and (c) **4Per-CN**. Blue and green surfaces represent α and β spin densities, respectively. Isovalue is 0.002.

thus best represented by the resonance of closed-shell Kekulé and biradical canonical forms as shown in Figure 1. Furthermore, this characteristic spin distribution pattern is found to be remarkable in the higher derivatives ($n > 3$), indicating that two terminal spin radicals are less electronic coupled due to the disruption of the effective π-bond character with the twisted orientations of rylene core units.

The fact of the larger singlet biradical character of **nPer-CN** would be also manifested by the bond elongations and dihedral angles between each perylene unit in the molecular structures. In comparison to the quinoidal **Per-CN** (Figure S5 in the Supporting Information), the singlet biradical **2Per-CN** and their higher ones showed longer bond lengths for the exo methylene bonds as the weakening of the C=C bonds was observed in vibrational studies. Upon an increase of the index y, dihedral angles of the singlet biradical **nPer-CN** between the NP cores are getting larger (55−64°) and close to that of the triplet biradical states (Figures S6, S8, S9 in the Supporting Information). Moreover, the determination of nucleus independent chemical shift (NICS) values[29] (e.g., NICS(1) and NICS(1)$_{zz}$) indicates more benzenoid character of the six-membered rings of the NP moieties in the singlet biradical species of **nPer-CN** as prolonging the molecular lengths (Figure S13 in the Supporting Information). These geometric findings suggest that the generation of aromaticity of rylene cores arising from biradical electronic structures would be one driving force to push the unpaired electrons out to the terminal edges of the molecules with breaking π bonds. In addition, the large strain arising from streric repulsion between the NP units in the quinoidal form can be partially released in the biradical form, which could be regarded as another importance driving force.

On the basis of the open-shell biradical nature of **nPer-CN** ($n = 2−6$), the characteristic low-lying excited states assigned by the admixing spin-associated (H, H → L, L) double excited electron configurations were identified by time-dependent BS-UB3LYP/6-31G(d,p) level calculations (Figure S14 in the Supporting Information). The lowest energy transitions (S$_0$ → S$_1$) are 0.98 eV (1210 nm, f = 0.0012) for **2Per-CN**, 1.12 eV (1109 nm, f = 0.0028) for **3Per-CN**, and 1.10 eV (1128 nm, f = 0.1863) for **4Per-CN**, respectively. The smaller energy gaps are consistent with the larger biradical character of **nPer-CN**, because a HOMO−LUMO gap is closely related to the

promotion of electrons from HOMO to LUMO. The other simulated transitions given by this UB3LYP method are consistent with the experimental spectra (Tables S1−S3 in the Supporting Information).

III. CONCLUSION

We have demonstrated an efficient method to prepare a series of soluble and stable extended benzoquinodimethanes oligomers **nPer-CN** (n = 1−6) with the conjugated benzoquinoid units longer than any other extended *p*-QDMs reported to date. Their electronic structure and geometry in the ground state were investigated by various experiments assisted by DFT calculations. Our results disclosed a clear chain-length dependence of the photophysical and electrochemical properties as well as magnetic properties. This series of molecules exhibited tunable ground-state structures, with **Per-CN** as a closed-shell hydrocarbon, **2Per-CN−4Per-CN** as open-shell singlet biradical species, and the higher order compounds **5Per-CN** and **6Per-CN** as triplet biradicals. Such a difference was caused by steric repulsion between the neighboring perylene units in the oligomers as well as the recovery of aromaticity of the quinoidal NP rings in the biradical forms, with the experimental evidence from Raman spectra and theoretical calculations. The unique nature of these oligomers in the ground state is responsive for the chain-length-dependent optical, electrochemical, and magnetic findings. Theoretical calculations helped to further understand the experimental observations. This series of compounds provide important information to understand the nature of chemical bonding and the fundamental chemical and physical phenomenon of largely extended quinoidal systems. Moreover, they are promising candidates for nonlinear optics, ambipolar field effect transistors, and organic spintronics due to their unique optical, electronic, and magnetic properties.

■ ASSOCIATED CONTENT

S **Supporting Information**
Synthetic procedures and characterization data of all other new compounds. Details for all physical characterizations and theoretical calculations. Additional spectroscopic and computational data. This material is available free of charge via the Internet at http://pubs.acs.org.

■ AUTHOR INFORMATION

Corresponding Author
chmwuj@nus.edu.sg; dongho@yonsei.ac.kr; casado@uma.es; msedingj@nus.edu.sg
Notes
The authors declare no competing financial interest.

■ ACKNOWLEDGMENTS

■ REFERENCES

(1) (a) Coulson, C. A.; Craig, D. P.; Maccoll, A.; Pullman, A. *Discuss. Faraday Soc.* **1947**, *2*, 36−38. (b) Szwarc, M. *Discuss. Fraraday Soc.* **1947**, *2*, 46−49. (c) Hush, N. S. *J. Polym. Sci.* **1952**, *11*, 289−298.

(2) (a) Thiele, J.; Balhorn, H. *Chem. Ber.* **1904**, *37*, 1463−1470. (b) Flynn, C. R.; Michl, J. *J. Am. Chem. Soc.* **1974**, *96*, 3280−3288.

(3) (a) Tschitschibabin, A. E. *Chem. Ber.* **1907**, *40*, 1810−1819. (b) Sloan, G. J.; Vaughan, W. R. *J. Org. Chem.* **1957**, *22*, 750−761. (c) Morozova, D. I.; Dyatkina, E. M. *Russ. Chem. Rev.* **1968**, *37*, 377−391. (d) Montgomery, L. K.; Huffman, J. C.; Jurczak, E. A.; Grendze, M. P. *J. Am. Chem. Soc.* **1986**, *108*, 6004−6011. (e) Porter, W. W., III; Vaid, T. P.; Rheingold, A. L. *J. Am. Chem. Soc.* **2005**, *127*, 16559−16566.

(4) Acker, D. S.; Hertler, W. R. *J. Am. Chem. Soc.* **1962**, *84*, 3370−3374.

(5) Maxfield, M.; Bloch, A. N.; Cowan, D. O. *J. Org. Chem.* **1985**, *50*, 1789−1796.

(6) (a) Hartzler, H. D. *J. Am. Chem. Soc.* **1964**, *86*, 2174−2175. (b) Addison, A. W.; Dalal, N. S.; Hoyano, Y.; Huizinga, S.; Weiler, L. *Can. J. Chem.* **1977**, *55*, 4191−4199.

(7) Casado, J.; Ortiz, R. P.; López Navarrete, J. T. *Chem. Soc. Rev.* **2012**, *41*, 5672−5686.

(8) (a) Gronowitz, S.; Uppström, B. *Acta Chem. Scand., Ser. B* **1974**, *28*, 981−985. (b) Suzuki, K.; Tomura, M.; Tanakaa, S.; Yamashita, Y. *Tetrahedron Lett.* **2000**, *41*, 8359−8364. (c) Fukushima, T.; Okazeri, N.; Miyashi, T.; Suzuki, K.; Yamashita, Y.; Suzuki, T. *Tetrahedron Lett.* **1999**, *40*, 1175−1178.

(9) (a) Pappenfus, T. M.; Chesterfield, R. J.; Frisbie, C. D.; Mann, K. R.; Casado, J.; Raff, J. D.; Miller, L. L. *J. Am. Chem. Soc.* **2002**, *124*, 4184−4185. (b) Chesterfield, R. J.; Newman, C. R.; Pappenfus, T. M.; Ewbank, P. C.; Haukaas, M. H.; Mann, K. R.; Miller, L. L.; Frisbie, C. D. *Adv. Mater.* **2003**, *15*, 1278−1282.

(10) (a) Takahashi, T.; Matsuoka, K. I.; Takimiya, K.; Otsubo, T.; Aso, Y. *J. Am. Chem. Soc.* **2005**, *127*, 8928−8929. (b) Ortiz, R. P.; Casado, J.; Gonzalez, S. R.; Hernandez, V.; Ortiz, R. P.; Casado, J.; Hernandez, V.; Navarrete, J. T. L.; Viruela, P. M.; Orti, E.; Takimiya, K.; Otsubo, T. *Angew. Chem., Int. Ed.* **2007**, *46*, 9057−9061.

(11) Sandman, D. J.; Garito, A. J. *J. Org. Chem.* **1974**, *39*, 1165−1166.

(12) Yanagimoto, T.; Takimiya, K.; Otsubo, T.; Ogura, F. *J. Chem. Soc., Chem. Commun.* **1993**, *6*, 519−520.

(13) (a) Chase, D. T.; Rose, B. D.; McClintock, S. P.; Zakharov, L. N.; Haley, M. M. *Angew. Chem., Int. Ed.* **2011**, *50*, 1127−1130. (b) Chase, D. T.; Fix, A. G.; Kang, S. J.; Rose, B. D.; Weber, C. D.; Zhong, Y.; Zakharov, L. N.; Lonergan, M. C.; Nuckolls, C.; Haley, M. M. *J. Am. Chem. Soc.* **2012**, *134*, 10349−10352.

(14) (a) Ohashi, K.; Kubo, T.; Masui, T.; Yamamoto, K.; Nakasuji, K.; Takui, T.; Kai, Y.; Murata, I. *J. Am. Chem. Soc.* **1998**, *120*, 2018−2027. (b) Kubo, T.; Sakamoto, M.; Akabane, M.; Fujiwara, Y.; Yamamoto, K.; Akita, M.; Inoue, K.; Takui, T.; Nakasuji, K. *Angew. Chem., Int. Ed.* **2004**, *43*, 7474−6479. (c) Kubo, T.; Shimizu, A.; Sakamoto, M.; Uruichi, M.; Yakushi, K.; Nakano, M.; Shiomi, D.; Sato, K.; Takui, T.; Morita, Y.; Nakasuji, K. *Angew. Chem., Int. Ed.* **2005**, *44*, 6564−6568. (d) Shimizu, A.; Uruichi, M.; Yakushi, K.; Matsuzaki, H.; Okamoto, H.; Nakano, M.; Hirao, Y.; Matsumoto, K.; Kurata, H.; Kubo, T. *Angew. Chem., Int. Ed.* **2009**, *48*, 5482−5486. (e) Shimizu, A.; Kubo, T.; Uruichi, M.; Yakushi, K.; Nakano, M.; Shiomi, D.; Sato, K.; Takui, T.; Hirao, Y.; Matsumoto, K.; Kurata, H.; Morita, Y.; Nakasuji, K. *J. Am. Chem. Soc.* **2010**, *132*, 14421−14428. (f) Shimizu, A.; Hirao, Y.; Matsumoto, K.; Kurata, H.; Kubo, T.; Uruichi, M.; Yakushi, K. *Chem. Commun.* **2012**, *48*, 5629−5631.

(15) (a) Sun, Z.; Ye, Q.; Chi, C.; Wu, J. *Chem. Soc. Rev.* **2012**, *41*, 7857−7889. (b) Umeda, R.; Hibi, D.; Miki, K.; Tobe, Y. *Org. Lett.* **2009**, *11*, 4104−4106. (c) Wu, T. C.; Chen, C. H.; Hibi, D.; Shimizu, A.; Tobe, Y.; Wu, Y. T. *Angew. Chem., Int. Ed.* **2010**, *49*, 7059−7062. (d) Sun, Z.; Huang, K.-W.; Wu, J. *Org. Lett.* **2010**, *12*, 4690−4693. (e) Sun, Z.; Huang, K.; Wu, J. *J. Am. Chem. Soc.* **2011**, *133*, 11896−11899. (f) Li, Y.; Heng, W.-K.; Lee, B. S.; Aratani, N.; Zafra, J. L.; Bao, N.; Lee, R.; Sung, Y. M.; Sun, Z.; Huang, K.-W.; Webster, R. D.; López Navarrete, J. T.; Kim, D.; Osuka, A.; Casada, J.; Ding, J.; Wu, J. *J. Am. Chem. Soc.* **2012**, *134*, 14913−14922.

(16) Kamada, K.; Ohta, K.; Kubo, T.; Shimizu, A.; Morita, Y.; Nakasuji, K.; Kishi, R.; Ohta, S.; Furukawa, S.-I.; Takahashi, H.; Nakano, M. *Angew. Chem., Int. Ed.* **2007**, *46*, 3544−3546.

(17) Chikamatsu, M.; Mikami, T.; Chisaka, J.; Yoshida, Y.; Azumi, R.; Yase, K. *Appl. Phys. Lett.* **2007**, *91*, 043506.

(18) Son, Y. W.; Cohen, M. L.; Louie, S. G. *Phys. Rev. Lett.* **2006**, *97*, 216803.

(19) Morita, Y.; Nishida, S.; Murata, T.; Moriguchi, M.; Ueda, A.; Satoh, M.; Arifuku, K.; Sato, K.; Takui, T. *Nat. Mater.* **2011**, *10*, 947−951.

(20) Zeng, Z.; Sung, Y.-M.; Bao, N.; Tan, D.; Lee, R.; Zafra, J.- L.; Lee, B.-S.; Ishida, M.; Ding, J.; López Navarrete, J.-T.; Li, Y.; Zeng, W.; Kim, D.-H.; Huang, K.-W.; Webster, R. D.; Casado, J.; Wu, J. *J. Am. Chem. Soc.* **2012**, *134*, 14513−14525.

(21) (a) Li, Y.; Wang, Z. *Org. Lett.* **2009**, *11*, 1385−1387. (b) Jiao, C.; Zhang, K.; Chi, C.; Wu, J. *Org. Lett.* **2009**, *11*, 4508−4511. (c) Jiao, C.; Huang, K.-W.; Guan, Z.; Xu, Q.-H.; Wu, J. *Org. Lett.* **2010**, *12*, 4046−4049. (d) Li, Y.; Gao, J.; Motta, S. I.; Negri, F.; Wang, Z. *J. Am. Chem. Soc.* **2010**, *132*, 4208−4213.

(22) Uno, M.; Seto, K.; Masuda, M.; Ueda, W.; Takahashi, S. *Tetrahedron Lett.* **1985**, *26*, 1553−1556.

(23) Bleaney, B.; Bowers, K. D. *Proc. R. Soc. London, Ser. A* **1952**, *214*, 451−465.

(24) (a) Casado, J.; Patchkovskii, S.; Zgierski, M. Z.; Hermosilla, L.; Sieiro, C.; Moreno Oliva, M.; López Navarrete, J. T. *Angew. Chem., Int. Ed.* **2008**, *47*, 1443−1446. (b) González, S. R.; Ie, Y.; Aso, Y.; López Navarrete, J. T.; Casado, J. *J. Am. Chem. Soc.* **2011**, *133*, 16350−16353.

(25) Zhu, L.; Jiao, C.; Xia, D.; Wu, J. *Tetrahedron Lett.* **2011**, *52*, 6411−6414.

(26) Zeng, W. D.; Lee, B. S.; Sung, Y. M.; Huang, K.-W.; Li, Y.; Kim, D.; Wu, J. *Chem. Commun.* **2012**, *48*, 7684−7686.

(27) Nakano, M.; Minami, T.; Yoneda, K.; Muhammad, S.; Kishi, R.; Shigeta, Y.; Kubo, T.; Rougier, L.; Champagne, B.; Kamada, K.; Ohta, K. *J. Phys. Chem. Lett.* **2011**, *2*, 1094−1101.

(28) Döýhnert, D.; Koutecký, J. *J. Am. Chem. Soc.* **1980**, *102*, 1789−1796.

(29) Chen, Z. F.; Wannere, C. S.; Corminboeuf, C.; Puchta, R.; Schleyer, P. V. *Chem. Rev.* **2005**, *105*, 3842−3888.